

# Threshold of complexity and Arnold tongues in Kerr ring microresonators

D.V. Skryabin,\* Z. Fan, A. Villois, and D.N. Puzyrev  
Department of Physics, University of Bath, Bath BA2 7AY, UK  
(Dated: submitted 04 April, 2020; published January 2021)

We show that the threshold condition for two pump photons to convert into a pair of the sideband ones in Kerr microresonators with high-quality factors breaks the pump laser parameter space into a sequence of narrow in frequency and broad in power Arnold tongues. Instability tongues become a dominant feature in resonators with the finesse dispersion parameter close to and above one. As pump power is increased, the tongues expand and cross by forming a line of cusps, i.e., the threshold of complexity, where more sideband pairs become unstable. We elaborate theory for the tongues and threshold of complexity, and report the synchronisation and frequency-domain symmetry breaking effects inside the tongues.

Arnold tongues [1, 2] is a well-known phenomenon in parametrically driven and coupled oscillator systems having cross-disciplinary applications [3]. The tongues appear as a sequence of the expanding instability and synchronisation intervals in the parameter space of the external drive frequency and amplitude. The Arnold-tongues concept established itself in neuroscience [4], structural [5] and nano-mechanics [6], quantum engineering [7–9] and in other areas. Periodicity embedded into the model equations is the key property underpinning the formation of Arnold tongues [1, 2]. Nonlinear effects in periodic optical systems have traditionally attracted considerable attention [10–12]. In particular, resonators that recirculate light and reinforce light-matter interaction are naturally suited to explore the interplay of periodicity, dissipative and nonlinear effects [12–18].

Arnold tongues emerge through the transformation of resonances of the underlying linear oscillator under the influence of dissipative and nonlinear effects. Hence, practical utilisation of this concept in resonators requires a robust control over the linewidth and mode-density. High-quality-factor microresonators are currently used in the state-of-art frequency conversion, precision spectroscopy, comb generation and single quanta manipulation [15–19]. These devices are few mm to few hundreds of nm long with the tens of GHz to THz resonance separations, i.e., free spectral ranges (FSRs), and finessees  $10^3$ - $10^6$ , that should be compared to the finessees  $\lesssim 10^2$  in fibre resonators [13, 14] and other modelocking devices [20]. High finesse is naturally accompanied by the relatively large finesse dispersion, which is a measure of the spectral non-equidistance and of the resonance density in the rotating frame, that play a critical role in bringing the microresonator Arnold-tongues to the physical realm.

The Lugiato-Lefever equation (LLE) [21] is a key model in the microresonator area [15]. Originally proposed in the context of pattern formation in an optical resonator supporting a single longitudinal and many transverse modes, it has since gained broad interdisciplinary significance [22]. A microresonator implementation of LLE (mLLE) describes the interaction of many longitudinal modes and therefore should reflect on the

forementioned connection between finesse and dispersion. Exploring an interplay of the two, we have found a broad range of parameters where a transition from the single-mode, i.e., continuous-wave (cw), operation to frequency conversion happens via the Arnold-tongue route. The mLLE Arnold-tongues structure emerges across the pump frequency range from the limit of the infinitesimal pump powers. Therefore a focus of this work is outside the hard excitation regimes, i.e., proximity of the upper state of the bistability loop, giving rise to the mLLE soliton modelocking [15, 23–28].

We show that the tongue tips are well separated if the finesse dispersion is the order of one, which implies that the regions of stable single-mode operation are first interleaved with the instability intervals where only one pair of sidebands with the mode numbers  $\pm\mu$  kicks off the frequency conversion process. As the pump is increased the tongues expand, at some point they start overlapping and form the complexity threshold. Above this threshold, two and more pairs of modes with different  $|\mu|$  are becoming unstable simultaneously. We elaborate a theory of the threshold of complexity and report nonlinear effects in its proximity. The term - *threshold of complexity* is inspired by the cellular automata related concepts and terminology [29].

We now introduce a model and explain how it maps onto physical devices, while more cross-area context is provided through the text and before summary. Amplitude  $\psi$  of the electric field in a ring microresonator can be expressed as a superposition of angular harmonics:  $\psi = \sum_{\mu} \psi_{\mu}(t)e^{i\mu\vartheta}$ . Here  $\mu$  and  $\psi_{\mu}$  are the mode numbers and amplitudes.  $\vartheta \in [0, 2\pi)$  is an angle varying along the ring. Resonant frequencies,  $\omega_{\mu}$ , are counted from  $\omega_0$  and approximated as

$$\omega_{\mu} = \omega_0 + D_1\mu + \frac{1}{2}D_2\mu^2, \quad \mu = 0, \pm 1, \pm 2, \dots \quad (1)$$

$D_1/2\pi$  is the resonator FSR, and  $D_2$  is the second order dispersion, characterising how FSR is changing with  $\mu$ . For example,  $D_1/2\pi = 15\text{GHz}$ ,  $|D_2|/2\pi = 1\text{kHz}$  are good estimates for  $\text{CaF}_2$  resonators for  $\omega_0/2\pi$  being close to 200THz pump,  $\omega_p$ , [30]. If  $\kappa/2\pi$  is the linewidth, then

the resonator finesse is

$$\mathcal{F}_\mu = \pm \frac{\omega_{\mu\pm 1} - \omega_\mu}{\kappa} = \mathcal{F} + \alpha_\mu, \quad \mathcal{F} = \frac{D_1}{\kappa}, \quad (2)$$

where we take  $+1$  for  $\mu > 0$  and  $-1$  for  $\mu < 0$ . Here,  $\mathcal{F}$  is the dispersion free finesse, and  $\alpha_\mu = \mathcal{F}_\mu - \mathcal{F}$  is the residual finesse,

$$\alpha_\mu = (\mu \pm \frac{1}{2})\mathcal{F}_d \approx \mu\mathcal{F}_d, \quad \mathcal{F}_d = \frac{D_2}{\kappa}. \quad (3)$$

$\mathcal{F}_d$  is the finesse dispersion, which is a key parameter in what follows. It can be either positive (anomalous dispersion,  $D_2 > 0$ ) or negative (normal dispersion,  $D_2 < 0$ ).  $Q = \omega_0/\kappa$  is the resonator quality factor.  $Q = 3 \cdot 10^9$ , which is a conservative number for  $\text{CaF}_2$  resonators, gives  $\kappa/2\pi = 67\text{kHz}$ ,  $\mathcal{F} = 22 \cdot 10^4$ , and  $|\mathcal{F}_d| \lesssim 1.5 \cdot 10^{-2}$  for these samples [30, 31]. For the high  $Q = 10^{11}$  samples [32],  $\kappa/2\pi = 2\text{kHz}$ ,  $\mathcal{F} = 750 \cdot 10^4$ , and  $|\mathcal{F}_d| \lesssim 0.5$ .

The Kerr mLLE is [23, 24, 33]

$$i\partial_t \psi = \delta_0 \psi - \frac{1}{2}D_2 \partial_\theta^2 \psi - i\frac{1}{2}\kappa(\psi - \mathcal{H}) - \gamma|\psi|^2 \psi. \quad (4)$$

Here,  $\mathcal{H}^2 = \frac{\eta}{\pi}\mathcal{F}\mathcal{W}$  is the intracavity pump power, where  $\mathcal{W}$  is the laser power.  $\eta = \kappa_c/\kappa < 1$  is the pump coupling efficiency and  $\kappa_c$  is the coupling rate.  $\gamma/2\pi = 10\text{kHz}/\mathcal{W}$  is the nonlinear parameter [33].  $\delta_0 = \omega_0 - \omega_p$  is detuning of the pump laser frequency,  $\omega_p$ , from  $\omega_0$ .

Transformation to the rotating reference frame,  $\theta = \vartheta - D_1 t$ , replaces the  $\omega_\mu$ -spectrum with the residual, i.e., mLLE, spectrum,

$$\frac{1}{\kappa}\Delta_\mu = \frac{1}{\kappa}\delta_0 + \frac{1}{2}\mu^2\mathcal{F}_d. \quad (5)$$

Respectively, the finesse  $\mathcal{F}_\mu$  is replaced with the residual finesse,  $\alpha_\mu$ , Eq. (3). The latter is also expressed as  $\alpha_\mu = \pm(\Delta_{\mu\pm 1} - \Delta_\mu)/\kappa$  and can be interpreted as the inverse mode density. Fig. 1(c) illustrates how the density of states in the residual spectrum is reduced with  $\mathcal{F}_d$  increasing, and also shows that the linear resonances,  $\Delta_\mu = 0$ , are located at  $\delta_0 < 0$  for  $\mathcal{F}_d > 0$ , and at  $\delta_0 > 0$  for  $\mathcal{F}_d < 0$ . Residual spectrum is non-equidistant, and hence, even for very small  $\mathcal{F}_d$ 's there always be a sufficiently large  $|\mu|$  making its resonances well separated. Thus,  $|\alpha_\mu| \ll 1$  and  $|\alpha_\mu| \gg 1$  correspond to the quasi-continuous and sparse limits of the residual spectrum, respectively. Note, that the finesse itself is maintained arbitrarily large in any case,  $\mathcal{F}_\mu \gg |\alpha_\mu|$ .

We now define the single-mode cw-solution of Eq. (4) as  $\psi = \sqrt{g/\gamma} e^{i\phi_0}$ , where  $g > 0$  solves

$$\gamma\mathcal{H}^2 = g + 4g(\delta_0 - g)^2/\kappa^2, \quad (6)$$

and recapture key steps in its stability analysis [21]. Perturbing the cw with a pair of sideband modes,  $\psi = \sqrt{g/\gamma} e^{i\phi_0} + \psi_\mu e^{i\mu\theta} + \psi_{-\mu}^* e^{-i\mu\theta}$ , we find  $i\partial_t \vec{q}_\mu = \widehat{V}_\mu \vec{q}_\mu$ , where  $\vec{q}_\mu = (\psi_\mu, \psi_{-\mu})^T$ , and

$$\widehat{V}_\mu = \begin{bmatrix} \Delta_\mu - 2g - i\frac{1}{2}\kappa & -ge^{i2\phi_0} \\ ge^{-i2\phi_0} & -\Delta_\mu + 2g - i\frac{1}{2}\kappa \end{bmatrix}. \quad (7)$$

Thus,  $g$  is simultaneously responsible for the nonlinear shifts of the resonances and the anti-Hermitian coupling between the  $\pm\mu$  sidebands. Setting  $\vec{q}_\mu \sim e^{\lambda_\mu t}$  gives [21]

$$\lambda_\mu(\lambda_\mu + \kappa) = 3(g_\mu^{(1)} - g)(g - g_\mu^{(2)}), \quad (8)$$

$$g_\mu^{(1),(2)} = \frac{2}{3}\Delta_\mu \pm \frac{1}{3}\sqrt{\Delta_\mu^2 - \frac{3}{4}\kappa^2}. \quad (9)$$

Degenerate four-wave-mixing (FWM) process described by  $\widehat{V}_\mu$  corresponds to the following photon energy conservation:  $2\hbar\omega_p = \hbar(\omega_p + \mu D_1 + \text{Im}\lambda_\mu) + \hbar(\omega_p - \mu D_1 - \text{Im}\lambda_\mu)$ . CW stability is neutral at  $\text{Re}\lambda_\mu = \lambda_\mu = 0$ ,

$$g = g_\mu^{(1)}, g = g_\mu^{(2)}. \quad (10)$$

Hence, FWM sidebands are exponentially amplified for  $g_\mu^{(2)} < g < g_\mu^{(1)}$ . Lower boundary of the cw stability in  $(\delta_0, \mathcal{H})$ -plane, i.e., the FWM-threshold, is made by the minima of  $g_\mu^{(2)}$  in  $\delta_0$ , which are found at  $\Delta_\mu = \kappa$ ,  $g_\mu^{(2)} = \kappa/2$  for every  $\mu$ . Explicitly, the corresponding intracavity pump power,  $\mathcal{H}_{\mu F}^2$ , and detuning,  $\delta_0^{(\mu F)} = \omega_0 - \omega_p^{(\mu F)}$ , along the FWM threshold is

$$\gamma\mathcal{H}_{\mu F}^2 = \frac{1}{2}\kappa[1 + (1 - \mu^2\mathcal{F}_d)^2], \quad (11)$$

$$\frac{1}{\kappa}\delta_0^{(\mu F)} = 1 - \frac{1}{2}\mu^2\mathcal{F}_d. \quad (12)$$

Eliminating  $\mu^2$  one finds

$$\gamma\mathcal{H}_{\mu F}^2 = \frac{1}{2}\kappa[1 + (1 - \frac{2}{\kappa}\delta_0^{(\mu F)})^2] \quad (13)$$

For  $\kappa = 2$ , Eqs. (12) and (13) match equations for  $a(n_c)$  and  $E_{Ic}$  from Ref. [21]. Here and below, the sub- and super-scripts  $F, C$  stand for the 'FWM' and 'Complexity' thresholds, respectively.

Eqs. (11), (12) represent a discrete set of values, while the laser power and frequency can be tuned continuously. Hence, the instability threshold in  $(\mathcal{H}, \delta_0)$  also exists between the discrete points with the coordinates specified by  $\delta_0^{(\mu F)}$  and  $\mathcal{H}_{\mu F}^2$ . To demonstrate if and when their separation is important, we substitute  $g = g_\mu^{(1)}$  and  $g = g_\mu^{(2)}$  directly to Eq. (6) and compute  $\mathcal{H}^2$  vs  $\delta_0$  for all  $\mu$ . This procedure returns, in general, an infinite number, one for each  $|\mu|$ , of threshold lines that are shown in Figs. 1(a),(b) for  $|\mathcal{F}_d| = 0.005$  and  $0.5$  ( $Q = 10^9$  and  $10^{11}$ ). For relatively small  $|\mathcal{F}_d|$  and quasi-continuous residual spectra, Fig. 1(c), the individual instability lines in Fig. 1(a) overlap tightly and form a visibly single threshold [24] reproduced by Eq. (13) with  $\mathcal{H}_{\mu F}$  vs  $\delta_0^{(\mu F)}$  considered as a continuous function.

As  $|\mathcal{F}_d|$  starts approaching 1 and if it goes above it, then resonances in the residual spectrum, Fig. 1(d), and the respective thresholds for the neighbouring  $|\mu|$  separate, so that the pump frequency and power range with FWM gain reshapes profoundly and forms instability tongues, Fig. 1(b). Now, Eq. (13) describes only the lowest power limit at which instability becomes possible, with the large areas of stability present above it,

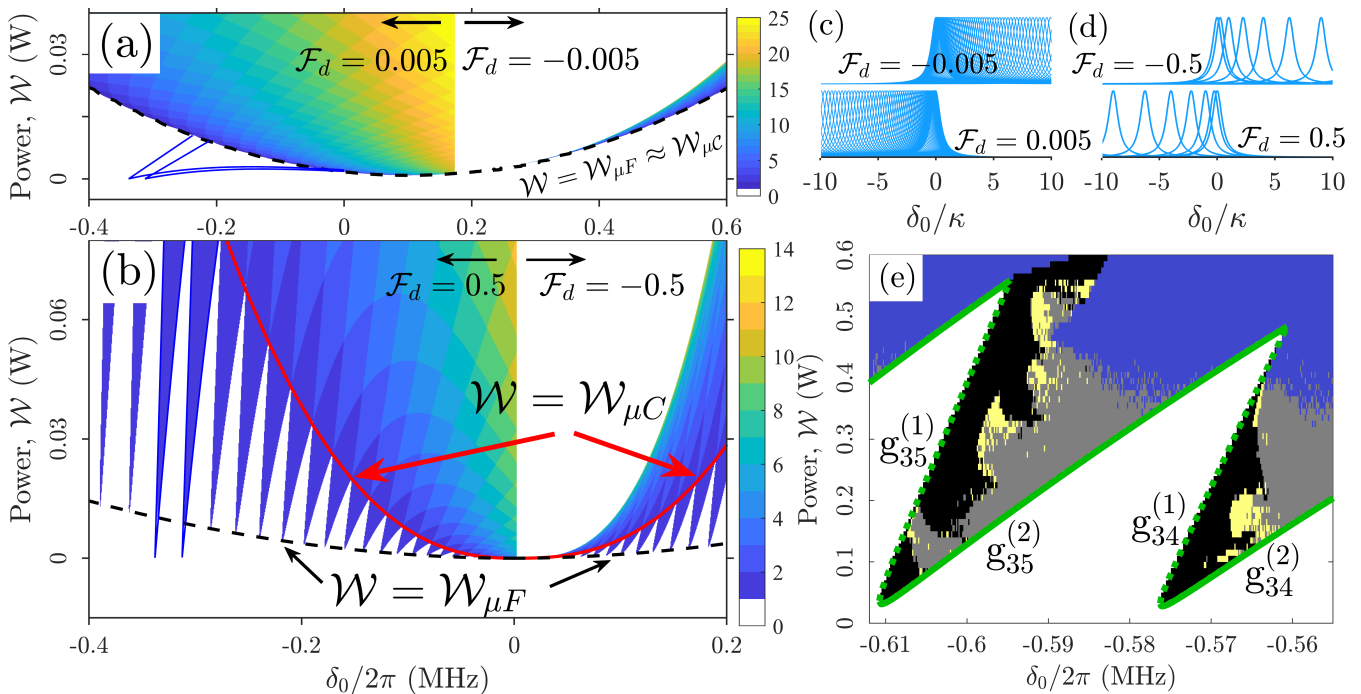


FIG. 1. **(a,b)** Arnold tongues and interplay of the FWM,  $\mathcal{W} = \mathcal{W}_{\mu F}$ , and complexity,  $\mathcal{W} = \mathcal{W}_{\mu C}$ , power thresholds for the quasi-continuous ( $|\mathcal{F}_d| = 0.005$ ,  $Q = 10^9$ ) and sparse ( $|\mathcal{F}_d| = 0.5$ ,  $Q = 10^{11}$ ) residual spectra;  $|D_2|/2\pi = 1\text{kHz}$ ,  $\eta = 0.5$ , residual finesse  $\mathcal{F}_d = D_2/\kappa = D_2Q/\omega_0$ . The color scheme shows the number of the simultaneously unstable  $\pm\mu$  sideband pairs. Lines dropping below  $\mathcal{W} = \mathcal{W}_{\mu F}$  and reaching  $\mathcal{W} = 0$  show a pair of the synchronisation tongues. **(c,d)** Resonances in the residual spectrum for small (c) and large (d)  $|\mathcal{F}_d|$ . Plots show Lorentzian lines,  $1/(1 + 4\Delta_\mu^2/\kappa^2)$ , for  $\mu$  starting from 0. **(e)** Distribution of the dynamical regimes across the  $|\mu| = 35$  instability tongue and its neighbourhood for  $\mathcal{F}_d = 0.5$ . Black color corresponds to the repetition rate locking to  $|\mu|D_1$ , see Fig. 2(a). Yellow marks the 'unlocked' regimes with the  $|d_\mu| = \text{const}$  symmetry breaking, see Fig. 2(b). Grey is the weak chaos with the symmetry breaking, see Fig. 2(c). Blue is the multimode complexity with dense continuous spectra, see Fig. 2(d). The intra-resonator cw power at the tongue minima  $g_{35}^{(2)}/\gamma = \kappa/2\gamma = 0.1\text{W}$  (FWM threshold), and  $g_{35}^{(1)}/\gamma = g_{36}^{(2)}/\gamma \simeq \alpha_{35}\kappa/2\gamma = 1.75\text{W}$  at the threshold of complexity.

see dashed black line in Fig. 1(b). We note, that  $\omega_p$ , in Figs. 1(a,b), is scanned across the narrow interval of  $10^{-4}D_1$  around  $\omega_0$  so that  $\omega_{\mu \neq 0}$  are not approached even remotely.

The instability tongues, when they are formed, provide selective excitation conditions for the sideband pairs with a given  $|\mu|$ . The tongue tips have been found along the quasi-linear tails of the  $g$  vs  $\delta_0$  solution of Eq. (6) for  $\delta_0 < \sqrt{3}\kappa/2 = \delta_b$  if  $\mathcal{F}_d > 0$ , and for  $\delta_0 > \delta_b$  if  $\mathcal{F}_d < 0$ . The tips are thus directly connected to the  $\Delta_\mu = 0$  resonances in the residual spectrum of the linear,  $g \rightarrow 0$ , resonator, see Fig. 1, Eq. (5), and more details below. The limiting value of  $\delta_0 = \delta_b$ , where the tongue structure diminishes, is found from  $g_0^{(1)} = g_0^{(2)}$ , which is the condition for the onset of bistability and the soliton regime ( $\mathcal{F}_d > 0$ ,  $\delta_0 > \delta_b$ ) [15]. Tongues have also been found by us in  $\text{Si}_3\text{N}_4$  resonators [34] with  $Q \sim 10^6 - 10^7$  [35, 36], and  $D_2 \sim 10^4\text{kHz}$ . The  $g = g_\mu^{(1)}$  (green squares in Fig. 1(e)) and  $g = g_\mu^{(2)}$  (green full lines) conditions shape the edges of the tongues, while their tips always belong to  $g = g_\mu^{(2)}$ .

Importantly, there is also a well-defined line that limits the area above the tongue tips and below their intersec-

tions, see red line in Fig. 1(b). We call this boundary - the threshold of complexity. Reaching this threshold signals two events. First is that the inter-tongue stability intervals cease to exist. Second is that the resonator is brought into the regime where  $\pm\mu$  and  $\pm(\mu + 1)$  sidebands can become simultaneously unstable. As the pump is increased further a sequence of thresholds, where more modes become unstable, can be seen in Figs. 1(a),(b). For smaller  $|\mathcal{F}_d|$  the residual spectrum is dense and all the thresholds tend to merge, while, for larger  $|\mathcal{F}_d|$ , their separation is pronounced.

Thus, the complexity threshold consists of the points where bifurcation lines corresponding to the excitations of the  $\pm\mu$ -sidebands intersect with the ones for  $\pm(\mu + 1)$ . Since  $\Delta_\mu$  is a function of  $\mu^2$ , assuming  $\mu > 0$  does not restrict the generality. Now, the intersection points, for  $\mathcal{F}_d > 0$ , can be found applying

$$g = g_\mu^{(2)} = g_{\mu+1}^{(2)}, \text{ and } g = g_\mu^{(1)} = g_{\mu+1}^{(2)}, \quad (14)$$

cf., Eq. (10). If  $\mathcal{F}_d < 0$ , then the second condition becomes  $g = g_\mu^{(2)} = g_{\mu+1}^{(1)}$ . Equations (14) is the mathematical quintessence of the complexity threshold. Each

of Eqs. (14) is a double, i.e., codimension-2, condition which marks a sequence of the instability points along the threshold line, see Fig. 1(b). Equations (14) are the cusp conditions and hence are non-differentiable in  $\delta_0$ , unlike  $g = g_\mu^{(2)}$ , Eqs. (10). For  $|\alpha_\mu| \ll 1$ ,  $|\mathcal{F}_d| \ll 1$ , the cusps become very shallow and the tongue structures disappear, while  $\mathcal{F}$  is still  $\gg 1$ .

Resolving Eqs. (14) gives

$$\Delta_\mu = \kappa \left( -\frac{1}{2}\alpha_\mu + \sqrt{1 + \alpha_\mu^2} \right). \quad (15)$$

The respective pump detunings are found applying Eqs. (5), (15),

$$\frac{1}{\kappa}\delta_0^{(\mu C)} = \left( -\frac{1}{2}\alpha_\mu + \sqrt{1 + \alpha_\mu^2} \right) - \frac{1}{2}\mu^2\mathcal{F}_d, \quad (16)$$

cf., Eq. (12).

If, e.g.,  $\alpha_\mu \gg 1$  ( $\mu \gg 1$ ,  $\mathcal{F}_d > 0$ ), then  $-\frac{1}{2}\alpha_\mu + \sqrt{1 + \alpha_\mu^2} = \frac{1}{2}\alpha_\mu + \mathcal{O}(\alpha_\mu^{-1})$ . Hence, Eq. (9) gives  $g = g_\mu^{(1)} \simeq \frac{1}{2}\kappa\alpha_\mu$  along the threshold of complexity. Simultaneously, the relatively large detunings,  $|\delta_0| \gg g$ , imply dispersive quasi-linear resonator response. E.g., for  $\kappa/2\pi = 2\text{kHz}$  ( $Q = 10^{11}$ ) and  $\mu = 35$ , we have  $\delta_0/2\pi \simeq 0.5\text{MHz}$  and  $g = g_{35}^{(1)} \simeq 2\pi \times 17\text{kHz}$  at the complexity threshold. Therefore, Eq. (6) can be approximated by  $\gamma\mathcal{H}^2 \simeq 4g\delta_0^2/\kappa^2$  and, hence, the laser power is

$$\mathcal{W}_{\mu C} \simeq \frac{\pi}{\eta\mathcal{F}} \frac{\kappa\mu^2}{2\gamma} |\alpha_\mu|^3 = \frac{\pi D_2^2}{2\gamma D_1} \frac{|\mu D_2|}{\eta\kappa} \mu^4, \quad |\alpha_\mu| \gg 1. \quad (17)$$

$\Delta_\mu = \kappa$  and  $g = g_\mu^{(2)} = \kappa/2$  at the FWM threshold, see Eq. (13), and hence  $\gamma\mathcal{H}^2 \simeq 4g\delta_0^2/\kappa^2$  now gives  $\mathcal{W}_{\mu F} = \mathcal{W}_{\mu C}/|\alpha_\mu| = \kappa\mathcal{W}_{\mu C}/|\mu D_2|$ . The prefactor that makes the difference between the powers at the FWM and complexity thresholds and hence measuring the relative depth of the instability tongues is exactly the residual finesse,  $\alpha_\mu$ .

The proximity of each tongue provides a parameter range where the mLLE dynamics is dominated by the competition between the two normal modes of  $\widehat{V}_\mu$ ,  $\widehat{V}_\mu \widehat{q}_\mu^{(\pm)} = i\lambda_\mu^{(\pm)} \widehat{q}_\mu^{(\pm)}$ . Rearranging Eq. (8) as  $(\lambda_\mu + \frac{1}{2}\kappa)^2 = (\Delta_\mu - g)(3g - \Delta_\mu)$ , we find  $\text{Im}\lambda_\mu^{(\pm)} = \pm \text{Im}\sqrt{3(\Delta_\mu - g)(g - \frac{1}{3}\Delta_\mu)}$ , and hence  $\text{Im}\lambda_\mu^{(\pm)} = 0$  is satisfied for  $\frac{1}{3}\Delta_\mu < g < \Delta_\mu$ . This is the normal mode synchronisation condition implying that the repetition rate of the emerging quasi-harmonic in  $\theta$ , i.e., roll, patterns locks to  $|\mu|D_1$ . While  $D_1$  is a property of the linear resonator and is independent of the pump parameters,  $\omega_p$  and  $g$ , the normal-mode synchronisation implies that the nonlinear,  $g \neq 0$ , repetition rate locks to an integer-multiple of  $D_1$ . The instability and synchronisation tongues merge together with  $|\mathcal{F}_d|$  increasing, and  $g_\mu^{(1)} \rightarrow \Delta_\mu$ ,  $g_\mu^{(2)} \rightarrow \frac{1}{3}\Delta_\mu$ , cf., Figs. 1(a) and (b) where two synchronisation tongues are contrasted against the instability ones.

Tongues are classified by their synchronisation order  $n : m$ , where  $n$  is the number of nonlinear pulses coming through the system per  $m$  periods of the linear oscillator [3]. In our case, the linear round trip time is  $2\pi/D_1$  and periods of the synchronised waveforms are  $2\pi/|\mu|D_1$ , thus the corresponding orders are  $|\mu| : 1$ . As for the classic Arnold tongues [3], the synchronization intervals start for infinitesimal pumps at the resonance points,  $\Delta_\mu = 0$ , in the linear,  $g \rightarrow 0$ , spectrum. The upper and middle branches of the  $g$  vs  $\delta_0$  curve inside the bistability interval (unlike its quasi-linear tails) do not withstand the  $g \rightarrow 0$  limit, and therefore their stability maps do not reveal the tongues.

Though the linear theory predicts  $|\mu| : 1$  synchronisation across the whole tongues area, the nonlinear processes make other regimes possible. The time-average mode frequencies are  $\tilde{\omega}_\mu = \omega_p + D_1\mu + \langle \partial_t \phi_\mu \rangle$ , where  $\phi_\mu(t) = \arg \psi_\mu$  [37]. Beating  $\psi_\mu$  against  $\psi_{-\mu}$  provides a measure of the average nonlinear repetition rate  $\tilde{D}_{1\mu} = \frac{1}{2}(\tilde{\omega}_\mu - \tilde{\omega}_{-\mu})$ . The difference between the two rates,  $\tilde{D}_{1\mu} - |\mu|D_1 = \frac{1}{2}(\langle \partial_t \phi_\mu \rangle - \langle \partial_t \phi_{-\mu} \rangle) \equiv |\mu|d_\mu$ , is a function of  $\omega_p$ , and  $g$ . Hence,  $d_\mu \neq 0$  implies desynchronisation, i.e., ‘unlocking’ of the repetition rate from  $|\mu|D_1$ .

Numerical simulations of Eq. (4) conducted for 20000 parameter points across the tongues have revealed that the locking,  $d_\mu = 0$ , range starts from the tongue tips and spreads along their  $g = g_\mu^{(1)}$  edges upwards, see black areas in Fig. 1(e), and Fig. 2(a). Another expressed feature of the dynamics inside the tongues is the violation of the repetition rate locking regimes producing  $d_\mu \neq 0$ , see yellow and grey areas in Fig. 1(e). In the coordinate space, the  $d_\mu \neq 0$  regimes correspond to a pair of the coexisting rolls rotating with the unlocked rates,  $|\mu|(D_1 \pm d_\mu)$ . Two rolls can either coexist independently (yellow areas), see one of them in Fig. 2(b), or generate chaotic switching dynamics (grey areas) associated with the weak modes emerging around the dominant ones, see Fig. 2(c). Here we deal with the frequency-domain symmetry breaking [42], when symmetry is broken not only for the sideband powers, see mode-number spectra in Figs. 2(b), but also for their spectral content, see and compare the radio-frequency (RF) spectra of the dominant modes in Figs. 2(a) and 2(b). As the threshold of complexity is approached and crossed, the few-mode dynamics is replaced by the transition to the developed multimode chaos, when every consecutive mode in the spectrum is excited forming very dense continua, see Fig. 2(d).

Before concluding, we make further contextual connections. Refs. [38, 39] looked at the similar to our problem of the Arnold tongue overlaps in dissipative maps and biological systems. Refs. [40, 41] measured synchronisation and tongues for the soliton sequences flowing across a fibre linking two micro-rings. Tongue formation studied by



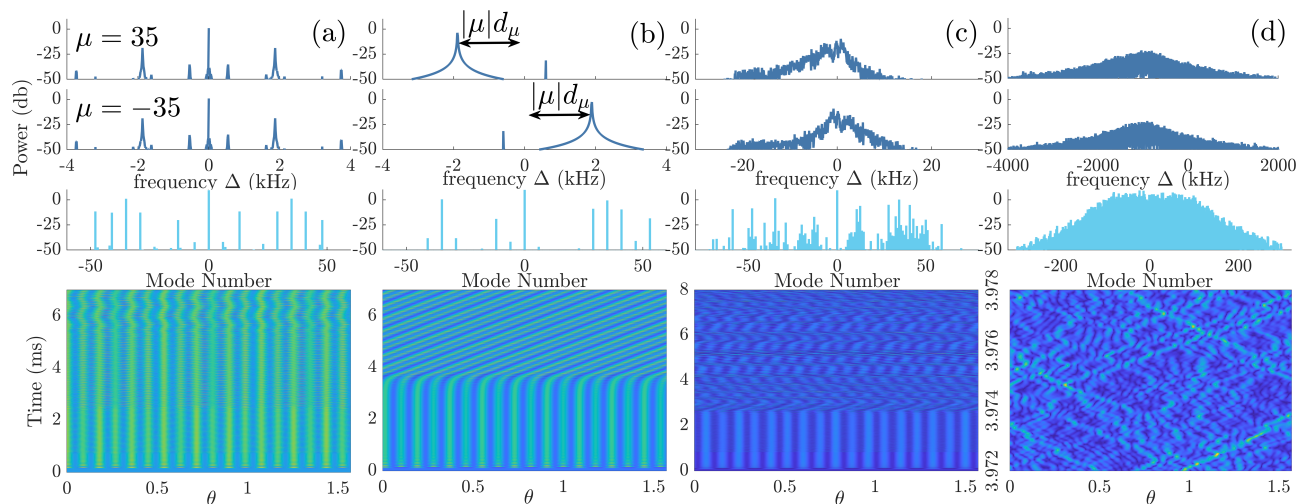


FIG. 2. **(a)** Repetition rate locking ( $d_\mu = 0$ , black area in Fig. 1(e)); **(b)** Frequency-domain symmetry breaking ( $d_\mu = \text{const}$ , yellow area in Fig. 1(e)); **(c)** Few-mode chaos (chaotic variations of  $d_\mu$ , grey area in Fig. 1(e)) **(d)** Multi-mode complexity (blue area in Fig. 1(e)). Top two rows show the  $\mu = \pm 35$  sideband RF spectra  $|S_\mu(\Delta)|^2$  [37]. 3rd row shows the mode powers at  $t = 16\text{ms}$ . 4th row is the space-time dynamics.

us should be compared with the multiple instability domains containing continua of modes reported in the zero finesse diffractive feedback systems [43], and in the low-finesse resonators [13, 14, 44]. Refs. [45–49] reported stationary and breathing rolls with no symmetry breaking in mLLE and alike systems. Refs. [42, 50, 51] studied symmetry breaking of the counter-propagating single-mode and soliton regimes in bi-directional microresonators.

In summary: We elaborated theory for the threshold of complexity and nonlinear effects within Arnold tongues in Kerr microresonators. Our results hold potential for applications in frequency conversion and RF-photonics areas relying on a range of existing and emerging high-Q resonators.

This work was supported by the EU Horizon 2020 Framework Programme (812818, MICROCOMB). We are deeply indebted to W.J. Firth and L.A. Lugiato for invaluable comments and interest in our work.

\* d.v.skryabin@bath.ac.uk

- [1] V. I. Arnold, Remarks on the perturbation problem for problems of Mathieu type, *Usp. Mat. Nauk*, **38** 189–203 (1983); *Russ. Math. Surveys*, **38**, 215–233 (1983).
- [2] V. I. Arnold, Small denominators and mappings of the circumference onto itself. *Izv. Akad. Nauk Ser. Mat.* **25**, 21–86 (1961); *AMS Transl. Ser. 2*, **46**, 213–284.
- [3] A. Pikovsky, M. Rosenblum, and J. Kurths, *Synchronization: A universal concept in nonlinear sciences* (Cambridge University Press, 2001).
- [4] M.M. Ali, K.K. Sellers, and F. Frohlich, Transcranial Alternating Current Stimulation Modulates Large-Scale Cortical Network Activity by Network Resonance, *J. Neuroscience* **33**, 11262 (2013).
- [5] G. W. Hunt and P. R. Everall, Arnold tongues and mode-jumping in the supercritical post-buckling of an archetypal elastic structure, *Proc. R. Soc. Lond. A* **455**, 125 (1999).
- [6] S.B. Shim, M. Imboden, and M. Pritiraj, Synchronized oscillation in coupled nanomechanical oscillators, *Science* **316**, 95 (2007).
- [7] T. E. Lee, C.-K. Chan, and S. Wang, Entanglement tongue and quantum synchronization of disordered oscillators, *Phys. Rev. E* **89**, 022913 (2014).
- [8] M. R. Jessop, W. Li, and A.D. Armour, Phase synchronization in coupled bistable oscillators, *Phys. Rev. Research* **2**, 013233 (2020).
- [9] N. Es’haqi-Sani, G. Manzano, R. Zambrini, and R. Fazio, Synchronization along quantum trajectories, *Phys. Rev. Research* **2**, 023101 (2020).
- [10] I.L. Garanovich, S. Longhi, A.A. Sukhorukov, and Y.S. Kivshar, Light propagation and localization in modulated photonic lattices and waveguides, *Phys. Rep.* **518**, 1 (2012).
- [11] K. Krupa, A. Tonello, A. Barthélemy, V. Couderc, B. M. Shalaby, A. Bendahmane, G. Millot, and S. Wabnitz, Observation of Geometric Parametric Instability Induced by the Periodic Spatial Self-Imaging of Multimode Waves, *Phys. Rev. Lett.* **116**, 183901 (2016).
- [12] D. W. Mc Laughlin, J. V. Moloney, and A.C. Newell, Solitary Waves as Fixed Points of Infinite-Dimensional Maps in an Optical Bistable Ring Cavity, *Phys. Rev. Lett.* **51**, 75 (1983).
- [13] F. Bessin, F. Copie, M. Conforti, A. Kudlinski, A. Mussot, and S. Trillo, Real-Time Characterization of Period-Doubling Dynamics in Uniform and Dispersion Oscillating Fiber Ring Cavities, *Phys. Rev. X* **9**, 041030 (2019).
- [14] N. Tarasov, A. M. Perego, D. V. Churkin, K. Staliunas, and S.K. Turitsyn, Mode-locking via dissipative Faraday instability, *Nat. Comm.* **7**, 12441 (2016).
- [15] T.J. Kippenberg, A.L. Gaeta, M. Lipson, and M. Gorodetsky, Dissipative Kerr solitons in optical mi-

- croresonators, *Science* **361**, eaan8083 (2018).
- [16] S.A. Diddams, K. Vahala, and T. Udem, Optical frequency combs: Coherently uniting the electromagnetic spectrum, *Science* **369**, eaay3676 (2020).
- [17] H. Kimble, The quantum internet, *Nature* **453**, 1023 (2008).
- [18] M. Kues, C. Reimer, J.M. Lukens, W.J. Munro, A.M. Weiner, D.J. Moss, and R. Morandotti, Quantum optical microcombs, *Nat. Phot.* **13**, 170 (2019).
- [19] Z. Vernon and J. E. Sipe, Strongly driven nonlinear quantum optics in microring resonators, *Phys. Rev. A* **92**, 033840 (2015).
- [20] U. Keller, Recent developments in compact ultrafast lasers, *Nature* **424**, 831 (2003).
- [21] L. A. Lugiato and R. Lefever, Spatial Dissipative Structures in Passive Optical Systems, *Phys. Rev. Lett.* **58**, 2209 (1987).
- [22] L. Lugiato, F. Prati, and M. Brambilla, *Nonlinear Optical Systems* (Cambridge University Press, 2015).
- [23] T. Herr, V. Brasch, J.D. Jost, C.Y. Wang, N.M. Kondratiev, M.L. Gorodetsky, and T.J. Kippenberg, Temporal solitons in optical microresonators, *Nat. Photon.* **8**, 145-152 (2014).
- [24] C. Godey, I.V. Balakireva, A. Coillet, and Y.K. Chembo, Stability analysis of the spatiotemporal Lugiato-Lefever model for Kerr optical frequency combs in the anomalous and normal dispersion regimes, *Phys. Rev. A* **89**, 063814 (2014).
- [25] Y. H. Wen, M. R. E. Lamont, S. H. Strogatz, and A.L. Gaeta, Self-organization in Kerr-cavity-soliton formation in parametric frequency combs, *Phys. Rev. A* **94**, 063843 (2016).
- [26] H. Taheri, P. Del'Haye, A. A. Eftekhar, K. Wiesenfeld, and A. Adibi, Self-synchronization phenomena in the Lugiato-Lefever equation, *Phys. Rev. A* **96**, 013828 (2017).
- [27] D. V. Skryabin and Y. V. Kartashov, Self-locking of the frequency comb repetition rate in microring resonators with higher order dispersions, *Opt. Express* **25**, 27442-27451 (2017).
- [28] D.C. Cole, A. Gatti, S.B. Papp, F. Prati, and L. Lugiato, Theory of Kerr frequency combs in Fabry-Perot resonators, *Phys. Rev. A* **98**, 013831 (2018).
- [29] S. Wolfram, *A New Kind of Science* (Wolfram Media, 2002).
- [30] A.A. Savchenkov, A.B. Matsko, V.S. Ilchenko, I. Solomatine, D. Seidel, and L. Maleki, Tunable Optical Frequency Comb with a Crystalline Whispering Gallery Mode Resonator, *Phys. Rev. Lett.* **101**, 093902 (2008).
- [31] I.S. Grudinin, N. Yu, and L. Maleki, Generation of optical frequency combs with a CaF<sub>2</sub> resonator, *Opt. Lett.* **34**, 878-880 (2009).
- [32] A. A. Savchenkov, A. B. Matsko, V.S. Ilchenko, and L. Maleki, Optical resonators with ten million finesse, *Opt. Express* **15**, 6768-6773 (2007).
- [33] D.V. Skryabin, Hierarchy of coupled mode and envelope models for bi-directional microresonators with Kerr nonlinearity, *OSA Continuum* **3**, 1364-1375 (2020).
- [34] D.N. Puzyrev, Z. Fan, and D.V. Skryabin, Modelling RF spectra of frequency combs (presented at Photon 2020, UK, 1-4 September 2020).
- [35] Z. Ye, K. Twayana, P. A. Andrekson, and V. TorresCompany, High-Q Si<sub>3</sub>N<sub>4</sub> microresonators based on a subtractive processing for Kerr nonlinear optics, *Opt. Express* **27**, 35719-35727 (2019).
- [36] H. El Dirani, L. Youssef, C. Petit-Etienne, S. Kerdiles, P. Grosse, C. Monat, E. Pargon, and C. Sciancalepore, Ultralow-loss tightly confining Si<sub>3</sub>N<sub>4</sub> waveguides and high-Q microresonators, *Opt. Express* **27**, 30726-30740 (2019).
- [37]  $\langle \partial_t \phi_\mu \rangle = \int \Delta |S_\mu|^2 d\Delta / \int |S_\mu|^2 d\Delta$ , where  $S_\mu(\Delta) = \tau^{-1} \int_{\tau_1}^{\tau_1+\tau} \psi_\mu(t) e^{i\Delta t} dt$ . The values of  $d_\mu$  used to separate the yellow and grey areas in Fig. 1(e) were also averaged over  $\tau_1$ .
- [38] M. H. Jensen, P. Bak, and T. Bohr, Transition to chaos by interaction of resonances in dissipative systems. I. Circle maps, *Phys. Rev. A* **30**, 1960 (1984).
- [39] M. Heltberg, R. A. Kellogg, S. Krishna, S. Tay, and M.H. Jensen, Noise Induces Hopping between NF-kB Entrainment Modes, *Cell Systems* **3**, 532-539 (2016).
- [40] J.K. Jang, A. Klenner, X.C. Ji, Y. Okawachi, M. Lipson, and A.L. Gaeta, Synchronization of coupled optical microresonators, *Nat. Photon.* **12**, 688 (2018).
- [41] J.K. Jang, X. Ji, C. Joshi, Y. Okawachi, M. Lipson, and A.L. Gaeta, Observation of Arnold Tongues in Coupled Soliton Kerr Frequency Combs, *Phys. Rev. Lett.* **123**, 153901 (2019).
- [42] D.V. Skryabin, A.G. Vladimirov, and A.M. Radin, Spontaneous phase symmetry-breaking due to cavity detuning in a class-A bidirectional ring laser, *Opt. Commun.* **116**, 109-115 (1995).
- [43] W. J. Firth, I. Kresić, G. Labeyrie, A. Camara, and T. Ackemann, Thick-medium model of transverse pattern formation in optically excited cold two-level atoms with a feedback mirror, *Phys. Rev. A* **96**, 053806 (2017).
- [44] Y.V. Kartashov, O. Alexander, and D.V. Skryabin, Multistability and coexisting soliton combs in ring resonators: the Lugiato-Lefever approach, *Opt. Express* **25**, 11550-11555 (2017).
- [45] L.A. Lugiato, C. Oldano, and L.M. Narducci, Cooperative frequency locking and stationary spatial structures in lasers, *J. Opt. Soc. Am. B* **5**, 879-888 (1988).
- [46] G.L. Oppo, M. Brambilla, and L.A. Lugiato, Formation and evolution of roll patterns in optical parametric oscillators, *Phys. Rev. A* **49**, 2028 (1994).
- [47] P. Parra-Rivas, D. Gomila, L. Gelens, and E. Knobloch, Bifurcation structure of periodic patterns in the Lugiato-Lefever equation with anomalous dispersion, *Phys. Rev. E* **98**, 042212 (2018).
- [48] A. Coillet, Z. Qi, I.V. Balakireva, G. Lin, C.R. Menyuk and Y.K. Chembo, On the transition to secondary Kerr combs in whispering-gallery mode resonators, *Opt. Lett.* **44**, 3078 (2019).
- [49] Z. Qi, S. Wang, J. Jaramillo-Villegas, M.H. Qi, A.M. Weiner, G. D'Aguzzo, T.F. Carruthers, and C.R. Menyuk, Dissipative cnoidal waves (Turing rolls) and the soliton limit in microring resonators, *Optica* **6**, 1220-1232 (2019).
- [50] M.T.M. Woodley, J.M. Silver, L. Hill, F. Copie, L. Del Bino, S. Zhang, G.L. Oppo, and P. Del'Haye, Universal symmetry-breaking dynamics for the Kerr interaction of counterpropagating light in dielectric ring resonators, *Phys. Rev. A* **98**, 053863 (2018).
- [51] W. Weng, R. Bouchand, E. Lucas, and T. J. Kippenberg, Polychromatic Cherenkov Radiation Induced Group Velocity Symmetry Breaking in Counterpropagating Dissipative Kerr Solitons, *Phys. Rev. Lett.* **123**, 253902

(2019).